npj | Quantum Information

www.nature.com/npjqi

ARTICLE OPEN

Long-range spin wave mediated control of defect qubits in nanodiamonds

Paolo Andrich[1], Charles F. de las Casas[1], Xiaoying Liu[1], Hope L. Bretscher[1], Jonson R. Berman[1], F. Joseph Heremans[1,2], Paul F. Nealey[1,2] and David D. Awschalom[1,2]

Hybrid architectures that combine nitrogen-vacancy centers in diamond with other materials and physical systems have been proposed to enhance the nitrogen-vacancy center's capabilities in many quantum sensing and information applications. In particular, spin waves in ferromagnetic materials are a promising candidate to implement these platforms due to their strong magnetic fields, which could be used to efficiently interact with the nitrogen-vacancy centers. Here, we develop an yttrium iron garnet-nanodiamond hybrid architecture constructed with the help of directed assembly and transfer printing techniques. Operating at ambient conditions, we demonstrate that surface confined spin waves excited in the ferromagnet can strongly amplify the interactions between a microwave source and the nitrogen-vacancy centers by enhancing the local microwave magnetic field by several orders of magnitude. Crucially, we show the existence of a regime in which coherent interactions between spin waves and nitrogen-vacancy centers dominate over incoherent mechanisms associated with the broadband magnetic field noise generated by the ferromagnet. These accomplishments enable the spin wave mediated coherent control of spin qubits over distances larger than 200 µm, and allow low power operations for future spintronic technologies.

npj Quantum Information (2017)3:28 ; doi:10.1038/s41534-017-0029-z

INTRODUCTION

In recent years, paramagnetic defects in semiconductors have fueled considerable advancements in the fields of quantum information and quantum sensing.[1–6] These developments were enabled, in great part, by the defects' remarkable spin coherence time,[7–11] which makes them very amenable qubit systems and is ultimately the result of their isolation from their environment. However, in many quantum sensing and information applications[5, 6, 12] it is desirable to increase the qubit's coupling to other degrees of freedom, such as other quantum bits or molecular spins, to improve the achievable quantum control and sensitivity. For this reason, hybrid quantum platforms, where materials or devices external to the defect's host are used to mediate the qubits' interactions, have recently emerged as a way to extend the capabilities of the spin qubits.[13, 14] In particular, a growing body of research has focused on the interplay between the optically addressable nitrogen-vacancy (NV) center in diamond and spin wave (SW) excitations in extended ferromagnetic materials.[15–19] These systems have been proposed, for instance, as a platform to enable long distance coupling between NV centers,[15] by taking advantage of the SW's long damping length and the large interactions achievable through the ferromagnet's (FM) sizeable magnetization.

However, a number of recent works[16–20] revealed that the coherences of NV centers placed in proximity of a FM are strongly quenched by the magnetic field noise generated by driven ferromagnetic resonances. These results are of great interest for the implementation of broadband magnetic field sensing and for the study of the spin properties of ferromagnetic systems, but also suggest that incoherent mechanisms dominate the SW-NV center coupling. Yet, the coherent nature of these interactions is critical, for instance, to use excitations in FMs as interaction buses between spin systems or to implement high-sensitivity metrology based on dynamical decoupling techniques.

In this work, we develop a hybrid yttrium iron garnet (YIG)-nanodiamond (ND) system integrating a thin YIG layer with a transparent, flexible, and transferable matrix with embedded NDs. We show that, under ambient conditions, surface confined Damon–Eshbach spin wave (DESW) modes excited in the YIG film using a microstrip line (MSL) antenna strongly interact with NV centers ensembles in NDs. Clear indications of the importance of the SWs' surface nature for the strong enhancement of the microwave-spin interactions is presented. Additionally, we demonstrate the existence of a microwave power regime where coherent coupling mechanisms between NV centers and SWs dominate over the effect of the FM's incoherent magnetic noise and we show that these coherent interactions are preserved over distances of up to 200 µm. While other recent efforts have successfully coupled NV centers to microscale FMs,[20, 21] geometries that can exploit the exceptionally long coherence lengths of propagating SWs are desirable to achieve, for instance, long-distance, tunable, coherent interactions in scalable systems. Moreover, leveraging the strongly enhanced SW-NV interactions we show that the microwave magnetic field of the antenna can be amplified by several orders of magnitude and can uniformly deliver this enhanced driving field hundreds of micrometers away from the MSL. These results suggest the possibility of using SW mediated interactions to enhance the microwave signature of spin targets to be sensed by the NV centers. Additionally, our system could enable the implementation of high-sensitivity widefield thermometry applications, which would greatly benefit from a

[1]Institute for Molecular Engineering, University of Chicago, Chicago, IL 60637, USA and [2]Materials Science Division, Argonne National Laboratory, Argonne, IL 60439, USA
Correspondence: David D. Awschalom (awsch@uchicago.edu)

Received: 22 June 2017 Revised: 24 June 2017 Accepted: 26 June 2017
Published online: 17 July 2017

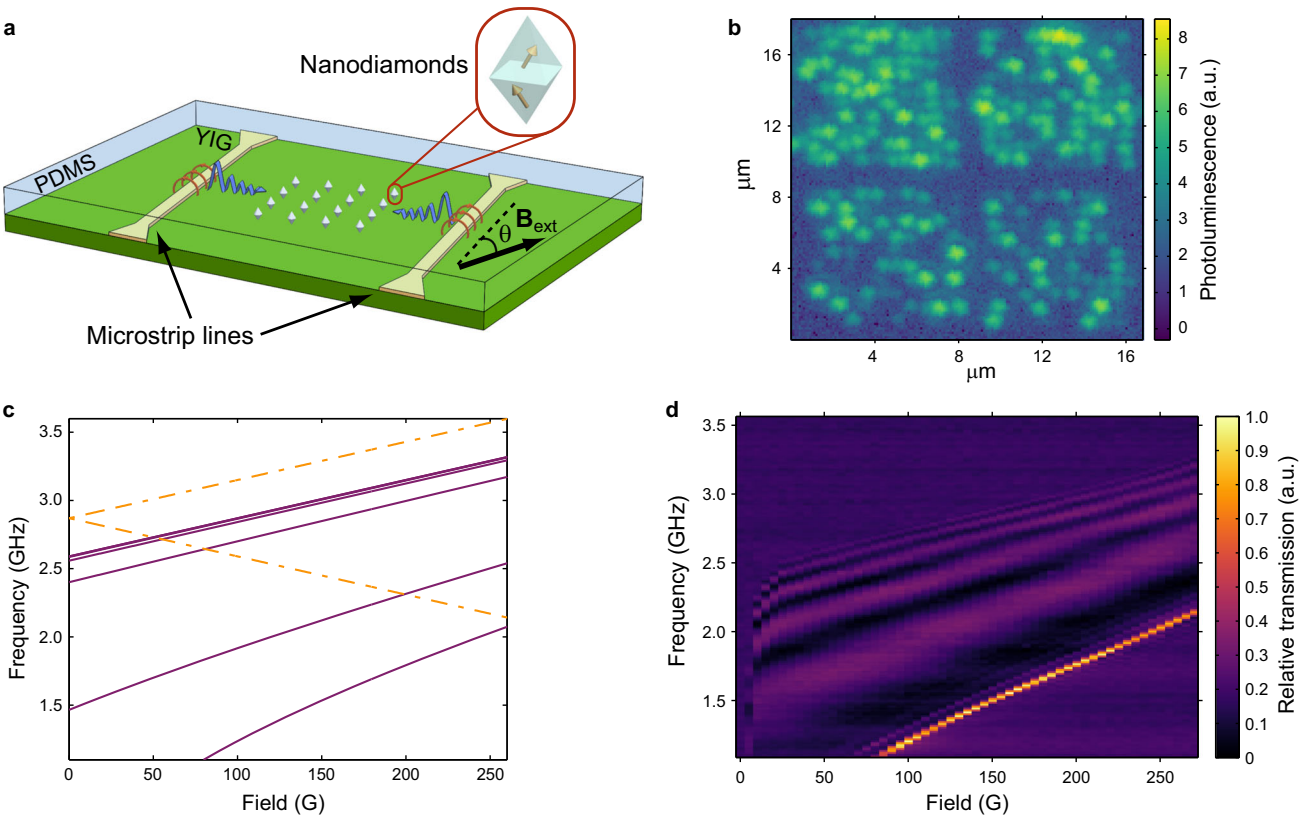

Fig. 1 Setup and dispersion relation of the surface confined spin wave modes. **a**, Sample schematics. The ferromagnetic layer is a 3.08 μm thick single-crystal YIG film epitaxially grown on a 500 μm GGG substrate. A ~300 μm thick PDMS strip with an array of NDs embedded on its surface is placed in contact with the YIG substrate. To apply and detect microwave fields, pairs of 5 μm wide microstrip lines (MSL) are patterned with different separations on the YIG. Microwave magnetic fields (*red circles*) and propagating spin waves (*purple lines*) are indicated. An external magnetic field (B_{ext}) is applied at an angle θ with respect to the MSLs. The arrows in the ND represent the NV center spins, with each ND containing hundreds of NV centers. **b**, Spatial photoluminescence scan of ND arrays collected using a confocal microscopy setup. **c**, Simulated SW spectrum of the YIG sample in the case of magnetic field parallel to the MSLs. The dashed lines enclose the range of frequencies where the NV centers' ground state spin resonances are located. **d**, Microwave transmission spectrum collected using two MSLs 100 μm apart as a function of the externally applied magnetic field for $\theta = 0$. The data for 0 G were subtracted from the data at higher fields to eliminate features that are not field dependent

reduction in the microwave power levels required to manipulate the NV centers, as these microwave signals can introduce heat in the system being probed.

RESULTS

Spin wave spectrum

To investigate the SW's properties and their interactions with NV centers we use the device geometry shown in Fig. 1a. MSLs fabricated on a YIG substrate are used to directly manipulate the NV centers' spin and to excite and detect SWs in the ferromagnetic layer. We employ a custom-built confocal microscopy apparatus to collect the photoluminescence from the NDs (see Fig. 1b), which are embedded in a polydimethylsiloxane (PDMS) matrix and positioned on the YIG surface.

As we are interested in the effects of the resonant interactions between SWs and NV centers, we first calculate and experimentally measure the SW spectrum of the FM to ascertain where it overlaps with the NV center's spin resonances. While the direction of the SW's propagation is always orthogonal to the MSL, SW modes with different properties can be excited depending on the relative orientation of the externally applied magnetic field B_{ext} and the direction of propagation of the SWs.[22] Here we primarily focus on DESWs (unless otherwise stated), which are excited when the external magnetic field is in the plane of the YIG film and parallel to the MSL (in particular we consider the direction that we identify as $\theta = 0$). We select these modes as their energies lie closest to the NV center spin ground state transitions at the magnetic fields used in this work ($B_{ext} = 0$ to 250 G) and we expect that their surface nature could provide the strongest interaction with external spins. We calculate the theoretical spectrum of the DESW following the approach detailed in Supplementary Note 2 and report the result of this calculation in Fig. 1c. In the same figure (*dashed lines*) we identify the frequency range for the NV center spin ground state resonances, which is enclosed by the resonance spectrum for a defect aligned with the external magnetic field. Even though the nanoparticles have random crystal orientations, their resonances inherently fall within this range.[23]

We also experimentally measure the SW modes dispersion using a network analyzer to collect microwave transmission measurements between two parallel MSLs separated by 100 μm.[24] In these measurements, a microwave signal is used to excite SWs at one of the MSLs, while the other antenna inductively detects the field generated by the propagating excitations (see Methods). The data in Fig. 1d, where the zero-field measurement is used as a reference for the ones at higher fields to eliminate the non-magnetic field dependent features, show good agreement with the calculated spectrum. Although the calculation does not capture all of the details in the measured spectra, this is likely the result of the necessarily simplified model for the MSL used to simulate the driving oscillating field. Nevertheless, this calculation confirms that the DESW modes are expected to be resonant with the NV center

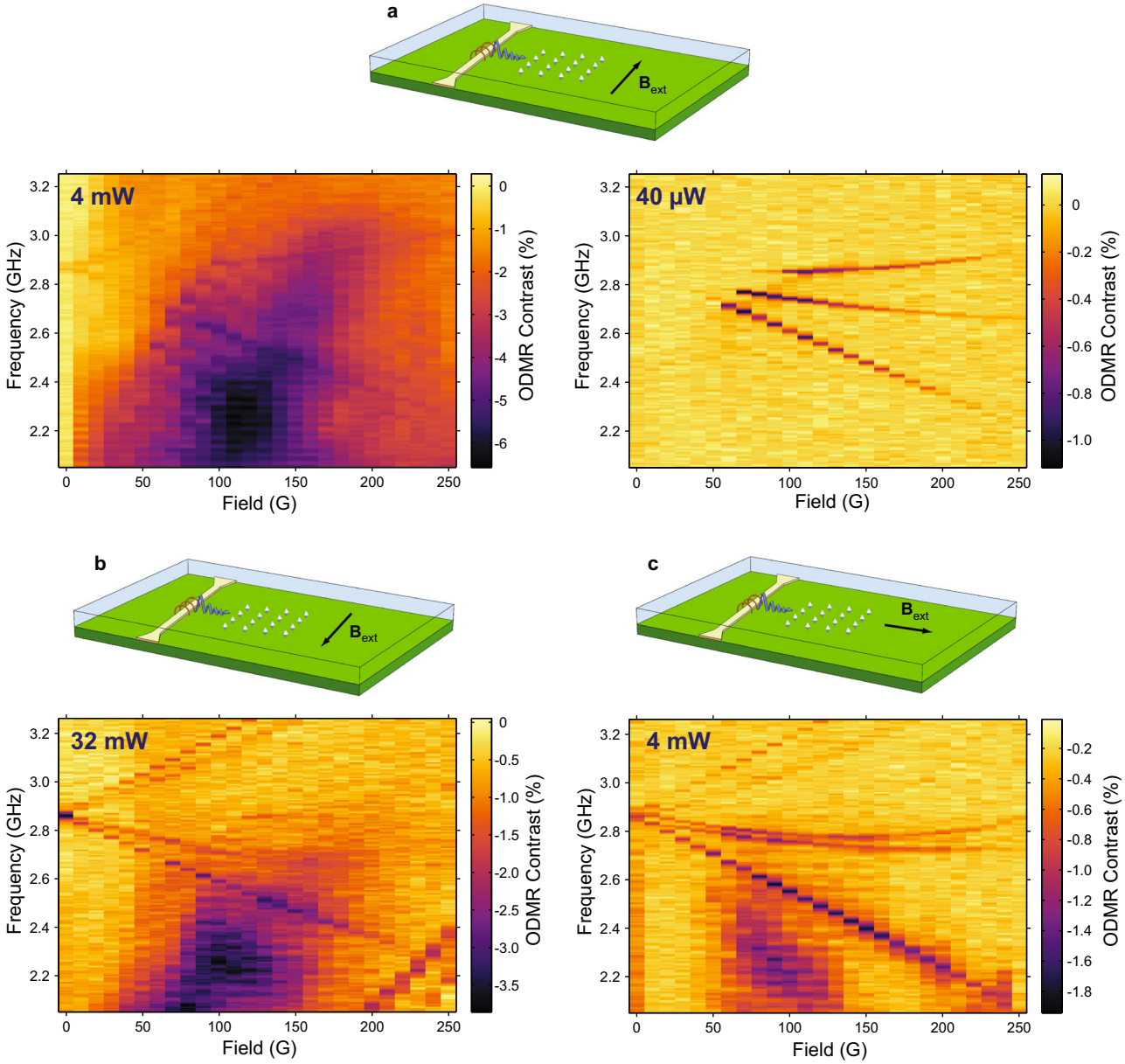

Fig. 2 Dependence of the ODMR spectra on microwave power and external magnetic field orientation. **a**, Spectra collected in the case of $\theta = 0$. In this condition, we excite DESW modes confined at the surface closest to the NDs. For a microwave power that allows us to resolve the ODMR resonance at zero field (*left*) a strong, broadband PL quenching is visible when the magnetic field is increased. By decreasing the microwave power by two orders of magnitude (*right*) we enter a regime where the non-resonant PL quenching is suppressed and discrete NV center resonances are visible at fields above 60 G. **b**, Spectra collected for $\theta = \pi$ using 32 mW of microwave power. In this condition, DESW are still excited, but the SW is now confined at the opposite surface of the YIG layer, resulting in the strong reduction in the PL quenching effect. **c**, Spectra collected for $\theta = \pi/2$ using 4 mW of microwave power. Here, we drive SW modes with sinusoidal profiles across the YIG layer. The absence of a strong surface confinement in the proximity of the NV centers results again in strongly diminished effects on the PL

transitions in the range of magnetic fields of interest. It is important to note in what follows that DESW excitations with higher frequencies (at a fixed external field) are associated with larger wave vectors k (Supplementary Note 2), and display a more pronounced surface confinement. In particular, both the magnetization oscillations within the ferromagnetic layer and the field generated outside decay exponentially with characteristic length $1/k$ in the direction orthogonal to the YIG surface.[22]

Optically detected resonant interaction

To study the extent of the DESW-NV centers interaction, we perform optically detected magnetic resonance (ODMR) measurements using one MSLs to drive microwave fields. Specifically, we detect changes in the NV centers' PL associated with the coupling of their spins to the antenna's or the SWs' oscillating magnetic field. Figure 2a shows the magnetic field configuration used for these measurements and the ODMR spectra obtained on a nanoparticle labeled NP-P, located ~40 μm away from the MSL. On the left, we report the results obtained using ~ 4 mW of microwave power, which is the lowest power that still resolves the NV center's resonances at low fields. When we increase the external magnetic field, we observe a broad feature of increasing frequency that intersects the NV center resonances following the SW modes' expected behavior. Recent studies have shown the presence of weaker off-resonant features in the NV

centers' ODMR spectrum[16, 18] ascribed to the shortening of the NV center longitudinal spin coherence time (T_1) caused by the broadband magnetic field noise introduced by the excited spin waves. Because of the extensive quenching effect on the spin coherence of the NV centers, it is not possible to isolate the effect of resonant interactions between the SWs and the spin qubits at this microwave power level.

When we instead decrease the input microwave power by two orders of magnitude (Fig. 2a, *right*), the off-resonant quenching is suppressed and we observe some of the NV centers discrete resonances. We observe that these resonances are visible only for magnetic fields above 60 G, which corresponds to the field at which we expect the resonances to intersect the SW modes (see Fig. 1c,d). The absence of optical contrast below this field, which corresponds to a lack of microwave driving of the NV centers, demonstrates that the effect of the antenna field is negligible at the ND location and that the NV center driving is purely SW mediated. We note that only the lower branches of the NV centers' ground state spin transitions are visible. We attribute this to the fact that the upper branches do not intersect the SW resonances, as can be inferred from Fig. 1c. The coarse magnetic field steps (10 G) used in these measurements is the reason we do not see the effect of separate SW excitations in the data of Fig. 2. When finer steps are taken, the discrete nature of the SW spectrum becomes clearly visible (Supplementary Note 4). Moreover, we note in Fig. 2a that the interaction appears to be stronger for the SWs associated with larger wave vectors, as can be deduced from the decrease in ODMR contrast at higher fields, where the NV centers' resonances cross lower k modes. This is consistent with a stronger surface confinement of the magnetization oscillations for higher values of k.

We observe strong SW-NV centers interactions on numerous nanoparticles using multiple MSLs and YIG substrates. As a control, ODMR measurements are collected also for NDs positioned on a gadolinium gallium garnet (GGG) non-magnetic substrate, where no off-resonant interactions nor enhanced resonant interactions are observed (Supplementary Note 9).

Dependence on the magnetic field orientation

In order to gain insight into the role the SW surface confinement plays in the strong coupling enhancement, we investigate the effect of the magnetic field orientation on the PL contrast for the cases $\theta = \pi$ and $\theta = \pi/2$. In these conditions, the excited SW have different dispersion relations and magnetization profiles, which allows us to analyze the dependence of the SW-NV interactions on these properties. In Fig. 2b we show the ODMR data collected for the $\theta = \pi$ case using 32 mW of microwave power, which is the minimum power needed to resolve the NV centers resonances at all fields. The strong reduction in the PL quenching with respect to the $\theta = 0$ case can be explained in light of the non-reciprocal nature of the DESW modes.[25] Indeed, a $\theta = \pi$ rotation of the magnetic field results in a decrease of the SWs' excitation efficiency[26, 27] and in a drastic change in the SWs amplitude profile, which is confined to the opposite surface of the ferromagnetic layer.[28]

In the case of $\theta = \pi/2$, pure backward volume magnetostatic spin waves (BVMSW) are excited.[22, 28] These modes have lower resonant frequencies (Supplementary Note 3) than the DESW and are characterized by a sinusoidal magnetization oscillation profile across the thickness of the ferromagnetic layer. In Fig. 2c we present the ODMR spectrum collected using 4 mW of microwave power. The extent to which the PL is affected is again remarkably smaller than for the $\theta = 0$ case. While the excitation efficiency for DESW and BVMSW can be different, this alone cannot explain the two orders of magnitude increase in power required to observe ODMR contrast in the latter case.[29] The difference in the frequencies of the two sets of modes also does not justify the absence of a region of strong PL quenching in the magnetic field range we studied, particularly considering the broadband nature of the off-resonant effects. Together, the measurements presented in Fig. 2 demonstrate the SW mediated nature of the enhanced microwave-NV center interactions and that the surface confinement of DESW is fundamental to this enhancement.

We note that these results suggest that tightly confined surface SW modes could provide a promising tool for the study of the spin properties of many nanoscale systems, similar to the way surface plasmons are used to investigate light-matter interactions.

Spin wave mediated coherent driving of NV centers

We now want to show that the strong resonant quenching of the NV centers' PL demonstrated above is the result of a coherent coupling mechanism between propagating SWs and NV centers. We demonstrate this through the observation of coherent Rabi oscillations of the NV centers driven by DESWs (Fig. 3a). The data were collected on an additional nanoparticle (NP-Q) at 120 G and

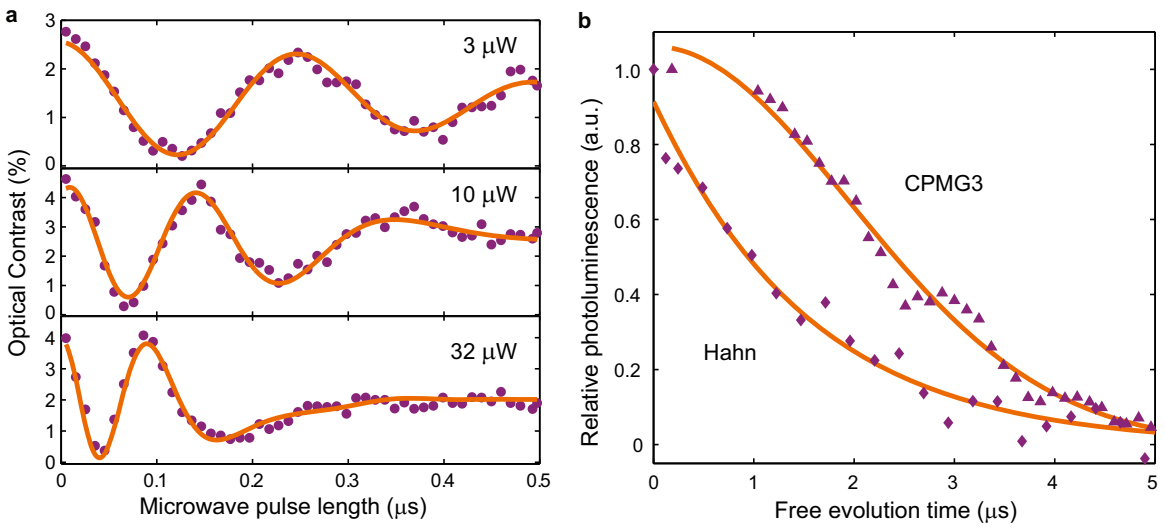

Fig. 3 Spin wave mediated coherent driving of NV centers. **a**, Rabi oscillations measured on NP-Q at a fixed external magnetic field (120 G) and different microwave powers. The nanoparticle is located 20 μm away from the driving MSL. **b**, Hahn-echo and Carr-Purcell-Meiboom-Gill 3π pulse (CPMG3) measurements that show robust multi-pulse control of the NV centers. Both sets of data are renormalized and fit to $\exp[-(t/T_2)^{\alpha}]$, where $\alpha = 1$ and 2 for the Hahn and CPMG3 case, respectively. From these fits we obtain $T_{2,Hahn} = 1.54$ μs and $T_{2,CPMG3} = 2.78$ μs

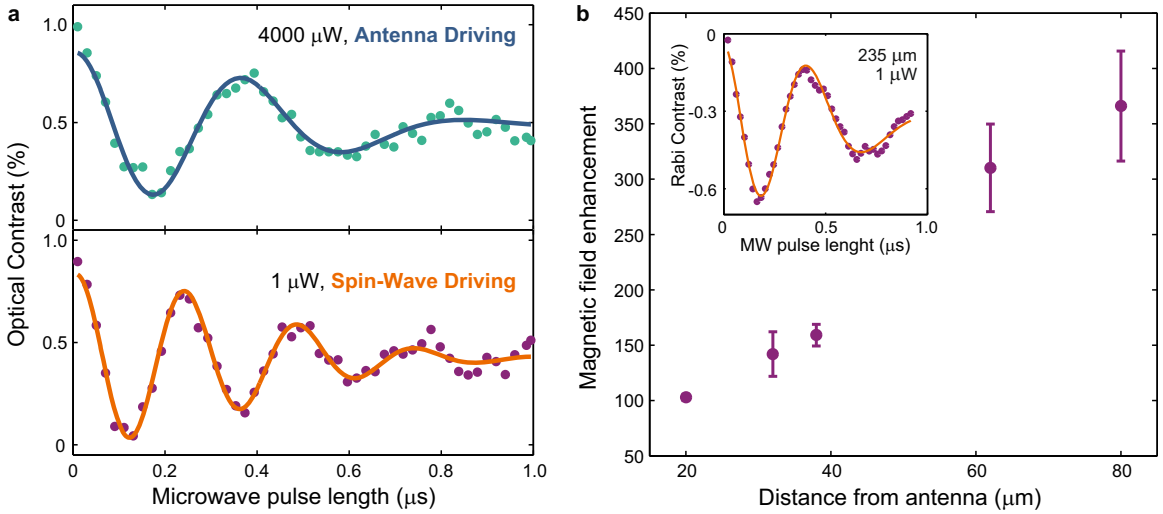

Fig. 4 Comparison of antenna and spin wave mediated coherent driving. **a**, Rabi oscillations measured on NP-Q (20 μm away from the MSL) at the same microwave driving frequency (2.862 GHz) but different external magnetic field and microwave power. The top curve is measured in the antenna driving regime at 15 G and using 4 mW of microwave power. The curve at the bottom is collected in the pure SW driving regime at 145 G and using 1 μW of microwave power. **b**, Microwave magnetic field enhancement as a function of the ND's distance from the antenna showing the effect of the long SWs damping lengths. The error bars reflect imprecisions in the determination of the Rabi frequencies. In the inset we show the Rabi signal obtained at high fields when the particle is ~235 μm away from the antenna using 1 μW of microwave (MW) power

at microwave powers where the antenna microwave field is negligible at the ND's location. The effect of the microwave power on the SW mediated coherent driving is also shown in Fig. 3a. The Rabi frequency increases linearly with the square root of the input power in the range used in this work (Supplementary Note 7), suggesting that we can neglect the impact of nonlinear effects.

We further demonstrate the robustness of the spin wave mediated coherent control using advanced multi-pulse dynamical decoupling protocols that are the basis for many high sensitivity metrology[3, 5, 6, 30] and quantum computing[12, 31] applications. In Fig. 3b we show the result obtained in the pure SW driving regime for another nanoparticle (NP-R) ~ 70 μm away from the MSL using ~5 μW of microwave power. The ability to extend the coherence time using multi-pulse sequences demonstrates full control of the NV centers through the pure SW driving. We note that, at the microwave power levels required to perform these measurements, the spin coherence times are not significantly altered by the presence of the ferromagnet, which is clear from measurements of T_2 on a ND first while in contact with YIG and then with a non-ferromagnetic GGG substrate (Supplementary Note 8). This result suggests that the NV centers' coherence properties are currently limited by the quality of the host material and not by the proximity to the FM, and can be extended using nanoparticles of higher qualities.[32, 33]

Enhancement of coherent microwave fields

Finally, we estimate the SW induced enhancement of the coherent microwave magnetic field that couples with the NV centers. To do this we compare the Rabi frequencies we obtain at low fields, where the SWs do not appreciably interact with the NV centers (antenna driving regime), with the Rabi frequencies at high fields and low powers (SW driving regime), where the direct antenna field is negligible at the nanoparticle's location. In order to isolate the effect of the SW mediated driving from other parameters that influence the SW-NV interaction, such as the frequency dependence of microwave power transmission and the NV center orientation, we focus again on nanoparticle NP-Q, which contains NV centers aligned nearly perpendicular to the external magnetic field. For these NV centers, the lower branch of the ground state spin transition can assume the same energy at low and high fields (Supplementary Note 5), which allows us to compare measurements collected from the same subset of the NV center ensemble using the same microwave frequency. In Fig. 4a we report the data collected at 15 and 145 G when NP-Q is 20 μm away from the MSL, which show that faster Rabi oscillations can be obtained in the SW driving regime using 1 μW of microwave power than in the antenna driving regime using 4 mW.

These results correspond to a SW mediated local enhancement of the driving microwave magnetic field by a factor of ~100 (Supplementary Note 6). This enhancement factor is a function of the nanoparticle's distance from the antenna as the antenna's field decays as the inverse of the distance while the magnetic field generated by the propagating SW is only limited by the YIG's large spin wave decay length.[24] This effect is illustrated in Fig. 4b where we show the behavior of the microwave magnetic field enhancement for NP-Q when we translate the ND from 20 to 80 μm away from the MSL. The enhancement increases roughly linearly to >350, which corresponds to five orders of magnitude less power required for the qubit driving and suggests that the SW decay length in this YIG substrate is significantly larger than 80 μm. To illustrate this point and to showcase the long-range nature of the SW-NV centers interaction we show the Rabi measurement (inset of Fig. 3b) collected ~235 μm away from the antenna using 1 μW of microwave power. This measurement was collected using a pair of MSLs separated by 300 μm to avoid the presence of an antenna along the SW propagation path, which could introduce damping in the propagating SWs. We note that at distances >80 μm, it becomes impossible to determine the enhancement factor as we do not observe direct driving induced by the antenna's electromagnetic field due to the limited microwave power available in our experiment.

Finally, we highlight that, even at very small distances from the antenna (lesser than approximately 100 nm), we obtain a large field enhancement of 30 ± 1.6 (see Supplementary Note 10). We note that the enhancement factor for a given separation depends on the magnetic field profile of the microwave source. For this reason, sources characterized by faster decaying fields, such as magnetic dipole moments, would benefit even more from the SW induced field amplification.

DISCUSSION

By using a hybrid YIG-ND quantum system to investigate the interactions between surface confined DESWs excited by a MSL and NV centers, we demonstrate the presence of a room temperature regime in which coherent coupling mechanisms can exceed the effects of incoherent interactions. This SW mediated coherent control persists at distances of more than 200 µm and is used to implement dynamical decoupling schemes on the NV centers' spins. Additionally, we show that DESWs can locally enhance the microwave magnetic field interacting with the NV centers by more than two orders of magnitude, which considerably lowers the amount of power needed for coherent control. These results have great significance in the efforts towards achieving enhanced sensing of small numbers of target spins as they suggest that surface confined SWs can very efficiently amplify the spins' microwave signature and transfer this amplified signal unchanged over large distances (Supplementary Note 11). Moreover, we note that the uniformity of the SW driving field has important implications for the development of widefield quantum sensing devices, where microwave signals need to be delivered homogeneously across a large array of sensors. In particular, the low power operation described here is suitable to perform sensitive temperature measurements, where microwave heating can interfere with naturally occurring thermal gradients. Finally, the strong, local microwave magnetic field enhancement obtained with DESWs could be of great interest to study the properties of spin systems at the nanoscale. We note that we achieve these results using inexpensive, commercially available nanoparticles, which makes our system highly scalable. Nevertheless, the use of engineered NDs with controllable NV center density, position, and orientation, as well as much improved coherence times,[32] could further the understanding of the SW-NV centers interactions. In particular, it could reveal the full potential of hybrid YIG-ND platforms for quantum information and sensing schemes while remaining compatible with the flexible polydimethylsiloxane (PDMS) membrane technique used here.

METHODS

The microwave signal for the direct manipulation of the NV centers and for spin wave (SW) excitation is provided by a signal generator (Stanford Research System Inc, SG396) and amplified through a broadband microwave amplifier (Mini-Circuits, TVA-11-422). The signal is then delivered to the sample through Ti/Au (8 nm/200 nm) MSLs patterned using an e-beam lithography process on a 3.08 µm thick YIG layer epitaxially grown on a GGG substrate (MTI Corp., YIG-GGG-100505). YIG is chosen as a substrate because of its small damping parameter for spin wave propagation in the GHz frequency range,[34] which makes it ideal for studying long-range interactions. The MSLs are tilted with respect to the sample edges to avoid SW reflections and are arranged at distances of 50, 100, and 300 µm to provide flexibility in our measurements. We use 4 mm long leads to the antenna in order to provide wire-bonding access outside the region covered by the PDMS layer. To minimize the loss in the microwave power delivered to the sample, the electrical leads are surrounded by two ground planes in a coplanar wave guide configuration that guarantees a good impedance match condition.

To perform the microwave transmission measurements one port of the network analyzer (Agilent Technologies, E8364B) is used to transmit the microwave signal to one of the MSLs, which generates an alternating Oersted magnetic field around the antenna. The components of this field orthogonal to the magnetization direction in the YIG exert a torque on the FM's magnetic moments, inducing their precession. These magnetic moments in turn generate a torque on their nearest neighbors and, when resonant conditions for the field and the microwave frequency are satisfied, the result is the excitation of SWs that propagate in the direction orthogonal to the MSL. Finally, the microwave field generated by the SW is inductively detected by the second MSL and the signal is collected at the second port of the network analyzer.

To complete the fabrication of the hybrid system we position in contact with the YIG layer an array of commercial NDs (Adamas Technology, ~500 NV centers per particle) embedded on the surface of a ~ 300 µm thick strip of PDMS. This architecture was fabricated through chemical pattern directed assembly[35] of NDs on a silicon substrate, followed by transfer printing[36] with PDMS as described in Supplementary Note 1. This portable and reusable system allows us to control the position of the NDs with respect to the MSLs and to easily locate and address single nanoparticles, which is critical for performing our measurements. Additionally, the flexibility of the PDMS guarantees the presence of close contact between the NDs and the YIG substrate.

The NV centers are optically excited using a 532 nm continuous-wave laser (Oxxius, 532S-150-COL-PP) and the emitted broadband fluorescence is isolated through appropriate band-pass filters and collected with a silicon avalanche photodetector (PerkinElmer, SPCM-AQR-13-FC). The home-built confocal microscope is equipped with a 0.6 NA objective with a 2.7 mm working distance (Nikon, CFI Plan Fluor ELWD 40xC) designed for coverglass correction in order to partially compensate for the aberrations introduced by imaging the NV centers through the PDMS layer. We introduce an acousto-optical modulator (Gooch & Housego, R35250-.2-.53-XQ) in the laser path to achieve the modulation of the optical excitation necessary in pulsed spin resonance measurements.

Data availability

The authors declare that the main data supporting the finding of this study are available within the article and its Supplementary Information files.

ACKNOWLEDGEMENTS

The authors thank B.B. Zhou and M. Fukami for useful discussions. This work was supported by the Army Research Office through the MURI program W911NF-14-1-0016 and U.S. Air Force Office of Scientific Research FA8650-090-D-5037. F.J.H., P.F.N. and D.D.A. were supported by the US Department of Energy, Office of Science, Basic Energy Sciences, Materials Sciences and Engineering Division.

AUTHOR CONTRIBUTIONS

P.A., C.F.D., and H.L.B. performed the experiments and completed the analysis of the data. X.L. and J.R.B. fabricated the nanodiamond arrays on PDMS. F.J.H, P.F.N., and D. D.A. advised and coordinated all efforts.

ADDITIONAL INFORMATION

Supplementary Information accompanies the paper on the *npj Quantum Information* website (doi:10.1038/s41534-017-0029-z).

Competing interests: The authors declare that they have no competing financial interests.

REFERENCES

1. Bernien, H. *et al*. Heralded entanglement between solid-state qubits separated by three metres. *Nature* **497**, 86–90 (2013).
2. Veldhorst, M. *et al*. A two-qubit logic gate in silicon. *Nature* **526**, 410–414 (2015).
3. Toyli, D. M., de las Casas, C. F., Christle, D. J., Dobrovitski, V. V. & Awschalom, D. D. Fluorescence thermometry enhanced by the quantum coherence of single spins in diamond. *Proc. Natl Acad. Sci. USA* **110**, 8417–8421 (2013).
4. Klimov, P. V., Falk, A. L., Christle, D. J., Dobrovitski, V. V. & Awschalom, D. D. Quantum entanglement at ambient conditions in a macroscopic solid-state spin ensemble. *Sci. Adv.* **1**, 1–8 (2015).
5. Mamin, H. J. *et al*. Nanoscale nuclear magnetic resonance with a nitrogen-vacancy spin sensor. *Science* **339**, 557–560 (2013).
6. Rugar, D. *et al*. Proton magnetic resonance imaging using a nitrogen-vacancy spin sensor. *Nat. Nanotechnol.* **10**, 120–124 (2015).
7. Balasubramanian, G. *et al*. Ultralong spin coherence time in isotopically engineered diamond. *Nat. Mater.* **8**, 383–387 (2009).
8. Christle, D., Falk, A. & Andrich, P. Isolated electron spins in silicon carbide with millisecond-coherence times. *Nat. Mater.* **14**, 160–163 (2014).
9. Widmann, M. *et al*. Coherent control of single spins in silicon carbide at room temperature. *Nat. Mater.* **14**, 164–168 (2015).
10. Pla, J. J. *et al*. High-fidelity readout and control of a nuclear spin qubit in silicon. *Nature.* **496**, 334–338 (2013).

11. Wolfowicz, G. *et al*. Atomic clock transitions in silicon-based spin qubits. *Nat. Nanotechnol*. **8**, 561–564 (2013).
12. Dolde, F. *et al*. Room-temperature entanglement between single defect spins in diamond. *Nat. Phys*. **9**, 139–143 (2013).
13. Li, P. B., Xiang, Z. L., Rabl, P. & Nori, F. Hybrid quantum device with nitrogen-vacancy centers in diamond coupled to carbon nanotubes. *Phys. Rev. Lett*. **117**, 1–7 (2016).
14. Kubo, Y. *et al*. Hybrid quantum circuit with a superconducting qubit coupled to a spin ensemble. *Phys. Rev. Lett*. **107**, 220501 (2011).
15. Trifunovic, L., Pedrocchi, F. L. & Loss, D. Long-distance entanglement of spin qubits via ferromagnet. *Phys. Rev. X* **3**, 041023 (2014).
16. Wolfe, C. S. *et al*. Off-resonant manipulation of spins in diamond via precessing magnetization of a proximal ferromagnet. *Phys. Rev. B* **89**, 180406(R) (2014).
17. Wolfe, C. S. *et al*. Spatially resolved detection of complex ferromagnetic dynamics using optically detected nitrogen-vacancy spins. *Appl. Phys. Lett*. **108**, 232409 (2016).
18. Page, M. R. *et al*. Optically Detected Ferromagnetic Resonance in Metallic Ferromagnets via Nitrogen Vacancy Centers in Diamond. Preprint at https://arxiv.org/abs/1607.07485 (2016).
19. Du, C. *et al*. Control and Local Measurement of the Spin Chemical Potential in a Magnetic Insulator. Preprint at https://arxiv.org/abs/1611.07408 (2016).
20. van der Sar, T., Casola, F., Walsworth, R. & Yacoby, A. Nanometre-scale probing of spin waves using single-electron spins. *Nat. Commun*. **6**, 7886 (2015).
21. Wolf, M. S., Badea, R. & Berezovsky, J. Fast, nanoscale addressability of nitrogen-vacancy spins via coupling to a dynamic ferromagnetic vortex. *Nat. Commun*. **7**, 5 (2015).
22. Stancil, D. D. & Prabhakar, A. *Spin Waves*. (Springer US, 2009).
23. Horowitz, V. R., Alemán, B. J., Christle, D. J., Cleland, A. N. & Awschalom, D. D. Electron spin resonance of nitrogen-vacancy centers in optically trapped nanodiamonds. *Proc. Natl Acad. Sci. USA* **109**, 13493–13497 (2012).
24. Yu, H. *et al*. Magnetic thin-film insulator with ultra-low spin wave damping for coherent nanomagnonics. *Sci. Rep*. **4**, 6848 (2014).
25. Schneider, T., Serga, A. A., Neumann, T., Hillebrands, B. & Kostylev, M. P. Phase reciprocity of spin-wave excitation by a microstrip antenna. *Phys. Rev. B* **77**, 214411 (2008).
26. Sekiguchi, K. *et al*. Nonreciprocal emission of spin-wave packet in FeNi film. *Appl. Phys. Lett*. **97**, 022508 (2010).
27. Demidov, V. E. *et al*. Excitation of microwaveguide modes by a stripe antenna. *Appl. Phys. Lett*. **95**, 112509 (2009).
28. Hurben, M. J. & Patton, C. E. Theory of magnetostatic waves for in-plane magnetized isotropic films. *J. Magn. Magn. Mater*. **139**, 263–291 (1995).
29. Serga, A. A., Chumak, A. V. & Hillebrands, B. YIG magnonics. *J. Phys. D: Appl. Phys*. **43**, 264002 (2010).
30. Mamin, H. J. *et al*. Multipulse double-quantum magnetometry with near-surface nitrogen-vacancy centers. *Phys. Rev. Lett*. **113**, 030803 (2014).
31. Gurudev Dutt, M. V. *et al*. Quantum register based on individual electronic and nuclear spin qubits in diamond. *Science* **316**, 1312–1316 (2007).
32. Andrich, P. *et al*. Engineered micro- and nanoscale diamonds as mobile probes for high-resolution sensing in fluid. *Nano. Lett*. **14**, 4959–4964 (2014).
33. Trusheim, M. E. *et al*. Scalable fabrication of high purity diamond nanocrystals with long-spin-coherence nitrogen vacancy centers. *Nano. Lett*. **14**, 32–36 (2014).
34. Sun, Y. *et al*. Damping in yttrium iron garnet nanoscale films capped by platinum. *Phys. Rev. Lett*. **111**, 106601 (2013).
35. Liu, X. *et al*. Deterministic Construction of Plasmonic Heterostructures in Well-Organized Arrays for Nanophotonic Materials. *Adv. Mater*. **27**, 7314–7319 (2015).
36. Carlson, A., Bowen, A. M., Huang, Y., Nuzzo, R. G. & Rogers, J. A. Transfer printing techniques for materials assembly and micro/nanodevice fabrication. *Adv. Mater*. **24**, 5284–5318 (2012).